Hydrogen sulfide removal from biogas by zeolite adsorption. Part II. MD simulations

Paolo Cosoli *, Marco Ferrone, Sabrina Pricl, Maurizio Fermeglia

Molecular Simulation Engineering (MOSE) Laboratory, Department of Chemical, Environmental and Raw Materials Engineering (DICAMP), University of Trieste, Piazzale Europa 1, 34127 Trieste, Italy

ARTICLE INFO

ABSTRACT

Coupled Grand Canonical-Canonical Monte Carlo and molecular dynamics (MD) simulation techniques have been used to investigate in details the adsorption of low-pressure hydrogen sulfide (H_2S) in zeolites, and the selective adsorption behavior towards carbon dioxide and methane, the main biogas constituents. Results from Monte Carlo (MC) simulations indicated, among many others, zeolite NaY as the best option for H_2S removal. Afterwards, deterministic simulations have been performed to investigate hydrogen sulfide pathway inside NaY, with respect to other adsorbed molecules (methane and carbon dioxide), as a function of zeolite loading and H_2S partial pressure (i.e., biogas composition). Thermodynamic evaluations for 2D molecular dynamic simulations in terms of binding energy evolution vs. time confirm and reinforce the results obtained from Monte Carlo simulations, testifying the greater affinity for H_2S to NaY zeolite framework. Results give also new quantitative insights in terms of pathways, binding energies, and equilibration time inside zeolite pores for stabilization.

© 2008 Elsevier B.V. All rights reserved.

1. Introduction

Nowadays biogas production and utilization is increasing, as it represents a renewable energy [1,2]. Nevertheless, there is a lot of interest for H_2S removal from biogas mixtures, as even low H_2S concentrations in atmosphere are harmful [1,3]; in fact, its concentration has to be dramatically reduced to the lower toxic limit (i.e., at least 10 ppm [1]). Among the possible solutions, one is the use of adsorption processes via hydrophilic, ion-rich zeolites [4–7]. Zeolite materials are particularly suitable for adsorption removal processes [8,9], by virtue of their high selectivity and compatibility towards polar compounds, such as H_2S [7,8].

The choice of the proper zeolite and the best operating adsorptive conditions can be refined by the helpful tool of molecular simulation techniques [10–12]. Grand Canonical Monte Carlo (GCMC) simulation techniques, such as those used in our recent publication [13], may give the possibility to choose the proper zeolite, and to evaluate its performances in terms of adsorption isotherms, both for H_2S only, and for H_2S in its biogas mixture (e.g., H_2S, carbon dioxide (CO_2) and methane (CH_4), essentially). With this aim, in our previous work [13] we have performed GCMC simulations at 298 K, with an increasing H_2S partial pressure ($P_{(H_2S)}$)

from 10 to 1000 Pa and at total pressure of 1 atm for both situations, being these compositions realistic for a biogas produced, for instance, by anaerobic digestion processes [1].

In this work we investigate in deeper details the results stemming from our previous GCMC simulations [13], which allowed us to choose the FAU NaY zeolite (Si/Al = 2.5) as the best one between NaY, NaX (Si/Al = 1), dealumined MFI and LTA (Si/Al = 1), in terms of H_2S removal. From these simulations it was clear that, increasing $P_{(H_2S)}$, there is a competition for adsorption sites between CH_4 and H_2S in polar zeolites (especially in NaY). This results in a reduction of CH_4 adsorption, while the CO_2 adsorbed quantity remains substantially unvaried. Our idea is to use molecular mechanics and dynamics simulations (MM/MD) to give more insights to the swapping phenomenon, investigating the behavior of already adsorbed molecules when the ensemble (NaY and adsorbed molecules) is perturbed by a new H_2S molecule which approaches the zeolite external surface. We simulated this dynamic, swapping-like behavior both for different biogas compositions inside zeolite framework, and for different zeolite loadings. We aimed at explaining and confirm the general trend arising from GCMC simulations from a thermodynamic and deterministic point of view.

2. Methods

All simulations have been carried out on an Intel bi-processor XEON 32bit workstation. We used *Sorption*, *Forcite* and *DMol*³

---

* Corresponding author. Tel.: +39 040 558 3757; fax: +39 040 569 823.
E-mail address: paolo.cosoli@dicamp.units.it (P. Cosoli).

Table 1
Non-bond terms in (NVT) MC simulations

Non-bond terms	Type	Accuracy (kcal/mol)	Cut-off (Å)	Truncation	Spline width (Å)
Electrostatic	Ewald and group	0.001	12.5	[–]	[–]
van der Waals	Atom based	[–]	12.5	Cubic spline	1

software modules of *Materials Studio* (v. 4.0, Accelrys, San Diego, CA, USA).

Details of Metropolis GCMC methods [14] employed in our research have already been described in details in previous works [12,13], and in many other publications [15–20], both for single and for multiple mixtures. The same applies to MM/MD classical methods to evaluate diffusion or permeation phenomena [21,19,22,23]. Accordingly, we will only briefly summarize below the aims and novelties of the procedure.

Adsorption isotherms for both pure H_2S and H_2S in a biogas mixture (CH_4, CO_2, H_2S) have been calculated for the following zeolites, in order to establish a list of priorities in terms of zeolite adsorption capacity and selectivity: MFI (dealumined), NaY (Si/Al = 2.5), NaX (Si/Al = 1) and LTA (Si/Al = 1) [24]. As in our previous paper, adsorbed molecules have been modeled by quantum-mechanics techniques, in the case of flexible H_2S, to determine bond lengths and angles under dynamic conditions, and partial charges, while CH_4 and CO_2 have been taken and represented with an all-atom model, with partial charges obtained from the selected *cvff_aug* force field. Then, the same Lennard-Jones parameters used in the first paper have been employed in all structures. MC simulations have been performed with the *cvff_aug* force field, at 298 K and a total constant pressure of 1 atm, being $P_{(H_2S)}$ held as a variable. Validation of the procedure has been obtained against experimental data [13]. We refer to Fig. 2, as taken from our previous paper [13], where the adsorption isotherms of pure H_2S and H_2S in biogas mixtures for all considered zeolites, and the relevant selectivity curves in Fig. 5 [13] are shown. As can be seen, the best porous material for H_2S removal is indeed zeolite NaY. The selectivity factor S_{ij} is defined as [16]

$$S_{ij} = \left(\frac{x_i}{x_j}\right)\left(\frac{y_j}{y_i}\right) \tag{1}$$

where x_i, x_j are the molar fractions of species i and j adsorbed in the zeolite, while y_i and y_j are the molar fraction of species i and j in the gas phase.

In this paper our aim is to confirm and investigate in greater details these results by the use of MC/MD coupled techniques. Many studies have been performed about self or corrected diffusion [25,26], and about preferential pathways of small molecules in zeolite pores [22,27]. The application of these methods seems quite difficult for our complex systems, both in terms of equilibrium dynamics and computing times [28], as Kinetic Monte Carlo techniques have been often indicated as the techniques of election. Basing our simulation procedures on previous MD techniques for similar systems [21,19,22,23,25–28], we looked for a correlation between the evident, more favorable tendency of H_2S to enter in NaY pores vs. the less favorable adsorption behavior exhibited by other molecules, especially the less polar CH_4.

To this purpose, we considered the behavior of an H_2S molecule which is approaching the zeolite surface when the NaY cell is already filled with adsorbed molecules (H_2S, CO_2, CH_4) at different loadings and at different $P_{(H_2S)}$. From previous MC adsorption isotherms calculations [13], we obtained the number of adsorbed molecules per cell at different $P_{(H_2S)}$. In Table 1 details of our MC simulations is exposed. In particular, we performed calculations for 1/3, 2/3 and full NaY cell coverage, at $P_{(H_2S)}$ of 10, 500 and 1000 Pa, with the number of molecules inserted approximated at the upper

integer number. Since the biogas pressure is 1 atm, and $P_{(H_2S)}$, as normally expected, is low (i.e., from 10 to 1000 Pa), we can sensibly take the vacuum as the external environment of the zeolite in our length scale of simulations. This means that the interactions between gas molecules are negligible in our model, and, thus, only one H_2S molecule is sufficient to describe the approaching and adsorption mechanisms of the molecule of interest.

The first step of our computational procedure is to run MC simulations in the Canonical Ensemble (NVT), with a fixed loading given by the relevant adsorption isotherms results. 10^6 trial steps, with 10^5 equilibration steps at 298 K have been performed, with the *cvff_aug* Force Field. The cut-off was fixed at 12.5 Å for both nonbonded energy terms (van der Waals and Coulomb interactions). For van der Waals terms we use a traditional atom based method. For electrostatic terms, the Ewald and group method has been used; in this method, interactions between charge groups are calculated using a group-based sum, while all other interactions are calculated using a Ewald sum.

Zeolite partial charges were assigned via the force field, while partial charges of molecules to be adsorbed have been taken from previous quantum-mechanics simulations (H_2S), or assigned by the force field (CH_4, CO_2) [13]. From these simulations, we considered the lowest final energy frames for each system for further considerations.

The 3D periodic cubic cells (25.1 Å for each side) have then been transformed into 2D periodic cells with a (0 0 1) cut plane (normal to z-axis), and then a new H_2S molecule has been inserted, as shown in Fig. 1. The molecule has been placed at the center of the cell length, at a distance of 2 Å from the NaY external surface. Although this is an arbitrary choice, the cell has a cubic symmetry, so the H_2S positioning is not affected by the choice of the cut plane. In this way, adsorbed molecules are free to change adsorption sites or to move outside the zeolite if the non-bonded interactions are less favorable, due to the disequilibrium imposed by the new H_2S molecule approach. The same H_2S molecule is free to move and position inside the cell, or to escape from the zeolite. The zeolite framework for all MD was kept fixed, while Na^+ ions and H_2S, CO_2 and CH_4 molecules had no constraints.
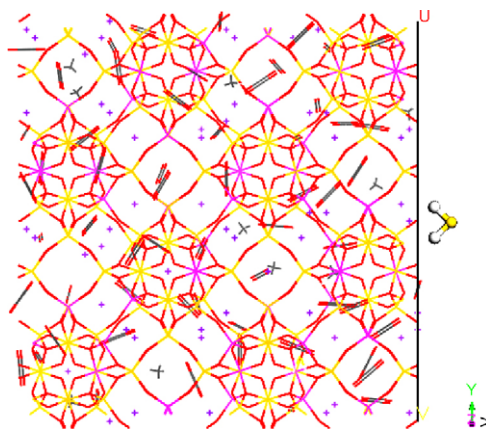

Fig. 1. 2D periodic cell of NaY structure with H_2S molecule approaching the framework.

Table 2
Details of the 2D dynamic simulations

	NVT	NVE
van der Waals	Atom based (cut-off = 18.5 Å)	Atom based (cut-off = 18.5 Å)
Coulomb	Ewald (accuracy = 10^{-5})	Ewald (accuracy = 10^{-5})
Thermostat algorithm	Velocity scale	–
Time step	1 fs	1 fs
Simulation time	20,000 ps	500,000 ps
Temperature	298 K	–
Frame sampling	Each 1000 ps	Each 1000 ps

Equilibration was performed with 20 ps of MD in the NVT ensemble, which allowed reaching sufficient energy stability in all simulations. NVT ensemble has been chosen for equilibration to preserve the cell morphology [29,30]. The last frames of NVT simulations have been used to start 500 ps of constant volume-constant energy (NVE) simulations, an ensemble which is usually more indicated to preserve the thermodynamics of the system [26,32–34], because if an external (artificial) thermostat is used, this will lead to an inevitable error of dynamics [35].

The details of NVT and NVE simulations are reported in Table 2; it should be noticed that the Ewald calculation method [31] was used for the calculation of the Coulomb energy component in the 2D periodic systems. The analysis of the MD simulations has been carried out considering:

- the number of molecules of each species escaping from the cell;
- the temporal evolution of molecules removal for each species;
- the binding energy evaluation for each species over time.

Binding energy analysis has been used in molecular simulation to evaluate thermodynamic behavior and stability of several complexes [36]. In a general case, given a complex of two generic molecules 1 and 2, the expression of the relevant energy of binding can be written as

$$E_{BIND(1,2)} = E_{1,2} - (E_1 + E_2) \tag{2}$$

where E_1, E_2 and $E_{1,2}$ are the total energies of the isolated molecules 1 and 2 and the complex, respectively. The calculation of E_1, E_2 is obtained by cancelling the other molecule(s) in a selected frame of MD. Given the method, the bond energy contributions cancel out in the difference (2), and only the non-bonded energy difference account for the binding energy term in physical complexes, as expected. If the value of E_{BIND} is negative, the complex is supposed to be thermodynamically favored while, on the contrary, the separation will be favored [37–40].

We considered five different ensembles in our simulation cell: the whole system itself, the zeolite framework (including Na$^+$ ions), and the adsorbed molecules (H$_2$S, CO$_2$, CH$_4$). In this way, the binding energies for H$_2$S, CO$_2$ and CH$_4$ have been calculated according to the following equation:

$$E_{BIND(ads,i)} = E_{TOTAL} - (E_{ads,i} + E_{ZEOL}) \tag{3}$$

where $E_{BIND(ads,i)}$ is the binding energy of the specific complex, E_{TOTAL} is the total energy of the whole system, $E_{ads,i}$ is the total energy of the specific adsorbed group of molecules, and E_{ZEOL} is the total energy of the zeolite alone. Binding energies have been analyzed for each different adsorbate, at different time steps, and taking into account molecular escape events. Binding energies have been then normalized by dividing $E_{BIND(ads,i)}$ for the number of molecules of the considered species inserted in the framework at the beginning.

3. Results and discussion

It was clear, even from the beginning of the NVT MD equilibrations, that the CH$_4$ molecules have a major tendency to escape from the framework, a phenomenon clearly related to their less polar characteristics. This confirms also the fact that hydrophilic zeolites, such as NaY, exhibit higher affinity for polar molecules (or molecules with a quadrupole moment, like CO$_2$). For this reason, the perturbation of the equilibrium, reached in the lowest energy frame of NVT-MC simulation, by a new H$_2$S molecule insertion tends decidedly to mobilize CH$_4$ molecules. Regarding CO$_2$ behavior, although its selectivity and isosteric heat of adsorption given by GCMC simulations is lower than that calculated for H$_2$S [13], it is not severely influenced by the perturbation: CO$_2$ molecules generally oscillate next to their adsorption sites, and their escaping tendency is very low. This can be ascribed to the fact that the quadrupole moment contributes to CO$_2$ binding stability, and to the planar, linear CO$_2$ shape, which allows the molecules to align inside the straight pores of NaY.

Quantitative results can be given both on terms of escaped molecules and in terms of binding energies. In Table 3 the list of total escaped molecules for each species is shown, while Fig. 2a–c shows escape events for each molecule in the NVE simulations. In this figure, each point represents escaping events at the given time step. It is important to note that we defined molecules as escaped when their center of mass is at a distance from the external zeolite surfaces greater than 12.5 Å. It may be observed that CH$_4$ molecules tend to exit rapidly from the cell along the z direction, as exemplified for example by the 3D visualizations of the 2D periodic simulation cell visualized in Fig. 3.
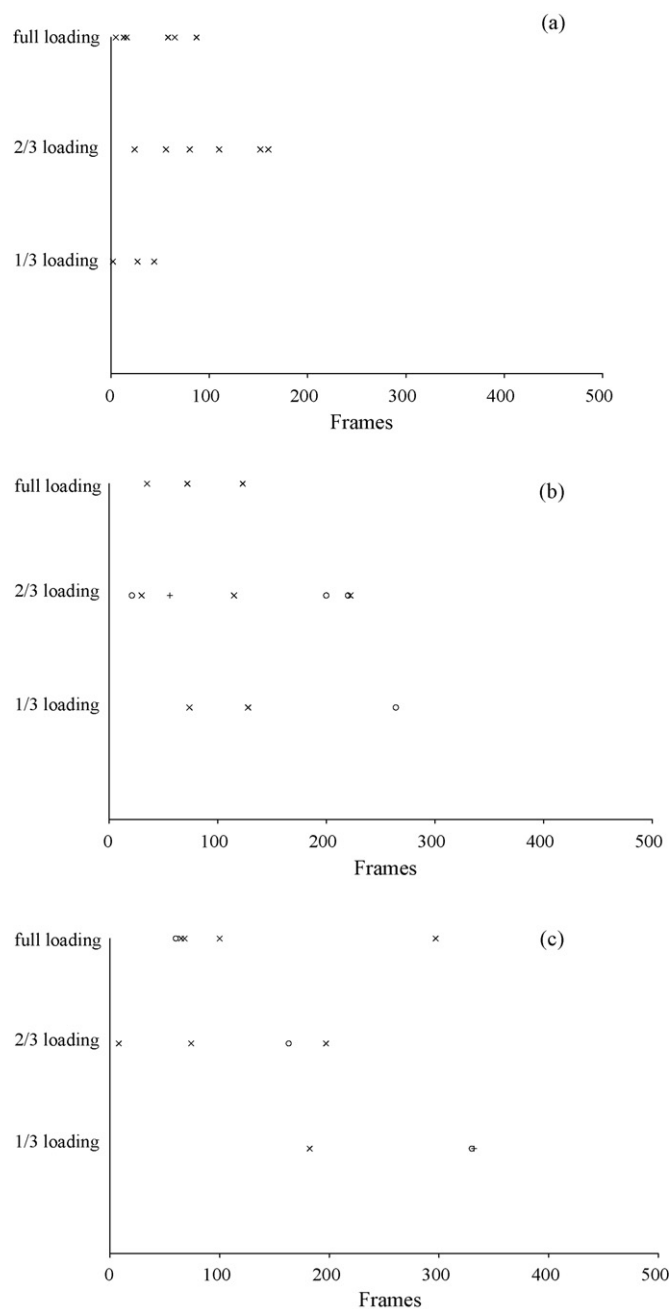
Table 3
Escaped molecules from NVT and NVE MD for different loading and different $P_{(H_2S)}$

Molecules	Loading = 1/3			Loading = 2/3			Full loading		
	CH$_4$	CO$_2$	H$_2$S	CH$_4$	CO$_2$	H$_2$S	CH$_4$	CO$_2$	H$_2$S
$P_{(H_2S)}$ = 10 Pa									
Initial number of molecules	3	19	0 (+1)	6	39	0 (+1)	10	59	1 (+1)
Escaped from NVT equilibration	0	0	0	1	0	0	2	2	0
Escaped from NVE simulation	3	0	0	4	0	0	6	0	0
$P_{(H_2S)}$ = 50 Pa									
Initial number of molecules	2	19	3 (+1)	3	39	7 (+1)	4	58	10 (+1)
Escaped from NVT equilibration	0	0	0	0	0	0	2	1	0
Escaped from NVE simulation	2	0	1	3	1	3	3	0	0
$P_{(H_2S)}$ = 1000 Pa									
Initial number of molecules	1	18	4 (+1)	3	36	9 (+1)	4	54	13 (+1)
Escaped from NVT equilibration	0	0	0	0	0	2	0	0	2
Escaped from NVE simulation	1	1	1	3	0	1	4	0	1

Fig. 2. Escaping molecules events for $P_{(H_2S)}$ of 10 Pa (a), 50 Pa (b), 1000 Pa (c); (×) CH$_4$, (+) CO$_2$, (○) H$_2$S. Each frame corresponds to 0.5 ps in NVE MD simulations.

The equilibrium condition is reached, in each case, well before 500 ps; only few H$_2$S and CO$_2$ molecules tend to escape. Generally, however, in correspondence of higher $P_{(H_2S)}$, and thus for higher H$_2$S fractions in the cell and for lower loadings (i.e., Fig. 2b and c), the equilibrium is reached more slowly. Although this behavior is difficult to explain, a tentative explanation might be related to the lower occupancy of free adsorption sites, especially for the few CH$_4$ molecules, which in these cases are allowed to cover longer pathways in relatively empty channels before finding the way to exit the framework.

It can also be noticed that, after molecule exits, the temperature of the system tends to increase (see additional information); this is reasonable, due to the acceleration of the escaping molecule. Both molecule pathways and temperature of the system always show stability within 350 ps, and none of the probe H$_2$S molecule inserted escapes from the cell.

Considering binding energies, we examined the binding energy behavior as a function of time (see Figs. 4–6). Each frame in these figures represents 0.5 ps of NVE MD simulation, and each binding energy value is averaged over the total number N of specific molecules inserted.

Although an attempt of fitting these curves is rather difficult or even impossible, these charts are helpful to explain adsorbed molecules behavior obtained by MD simulations. Binding energy evolutions are obviously influenced by molecule exit events; for instance, by considering the MD trajectory of the case shown in Fig. 4b, one CH$_4$ molecule escapes at frame 66, comes back at frame 80, and then leaves the zeolite again at frame 148. As can be seen from Fig. 4b, the corresponding binding energy trend clearly reflects this behavior. In general, all trends dramatically confirm the high speed with which methane tend to move out from the zeolite. Only when $P_{(H_2S)}$ = 10 Pa, and thus the number of H$_2$S molecules is low, some CH$_4$ molecules remain in the zeolite framework, but generally they all escape before 300 ps. Indeed, values of E_{BIND} = 0 kcal mol^{-1} N^{-1} mean that all CH$_4$ molecules are dispersed outside the cell at a distance higher than imposed cut-offs. Generally, it appears that H$_2$S binding energies per molecule are considerably higher than those of CH$_4$; CO$_2$, on the other hand, shows the most stable behavior and, generally, is characterized by the most favorable binding energy.

This analysis contributes to explain also the adsorption behavior at different H$_2$S pressures [13]; when $P_{(H_2S)}$ is increased, an adsorption competition process takes place, resulting in a swap of adsorption sites between H$_2$S and CH$_4$ molecules; accordingly, the H$_2$S adsorption increases. Nevertheless, selectivity S_{H_2S,CH_4} is much more enhanced at low H$_2$S pressures (i.e., lower loadings) due to the fact that more energetically suitable and free pores are available for H$_2$S. Thus, examining local binding energy evolution, e.g. immediately before and after CH$_4$ molecules leave the framework, an interesting behavior can be noticed (see Table 4). We considered only
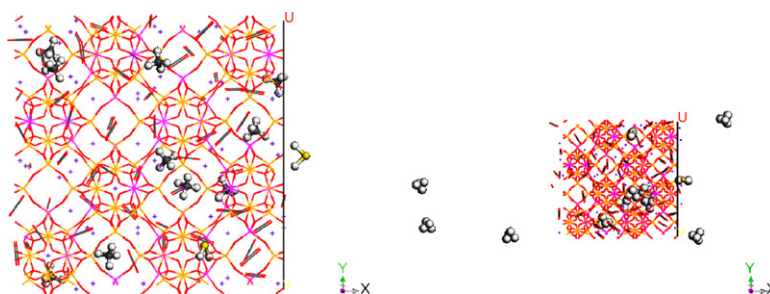

Fig. 3. 3D visualization of a 2D periodic cell at initial conditions (left) and after 6 ps of MD simulation (NVE ensemble, right); $P_{(H_2S)}$ = 10 Pa, full loading. The methane molecules escaping from the cell are represented in gray-and-white CPK representation.

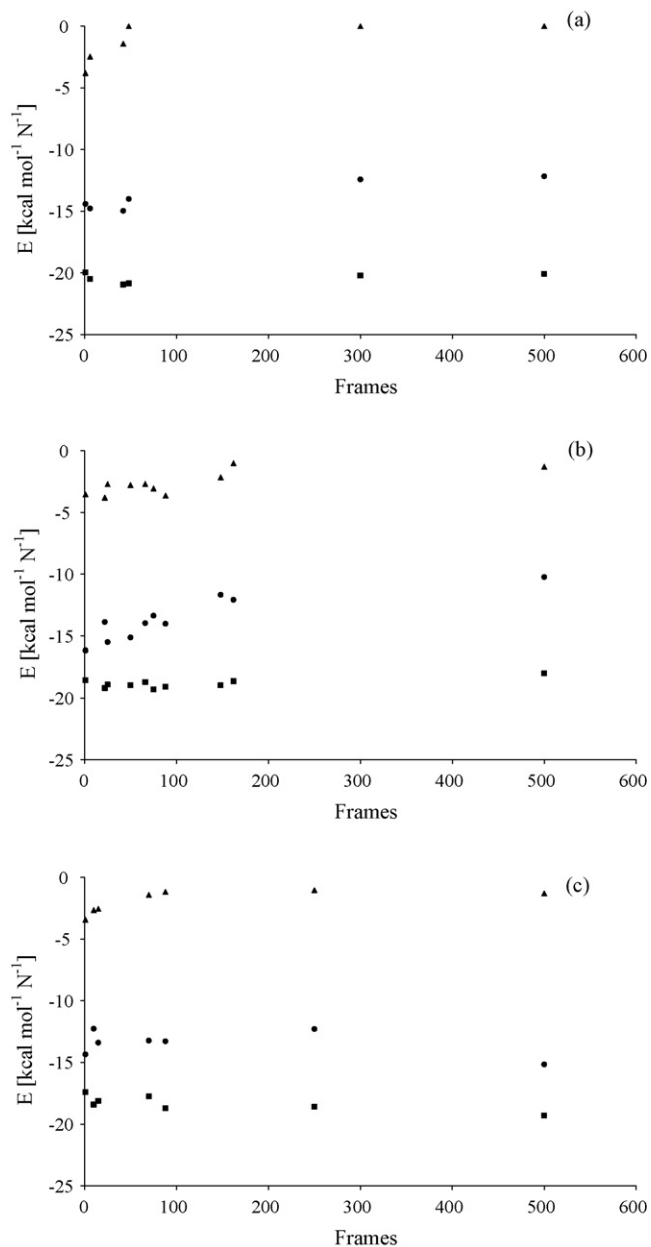**Fig. 4.** Binding energies as a function of time frames for NVE MD simulations at $P_{(H_2S)} = 10$ Pa; (a) 1/3 loading, (b) 2/3 loading, (c) full loading; (●) H_2S, (■) CO_2, (▲) CH_4.

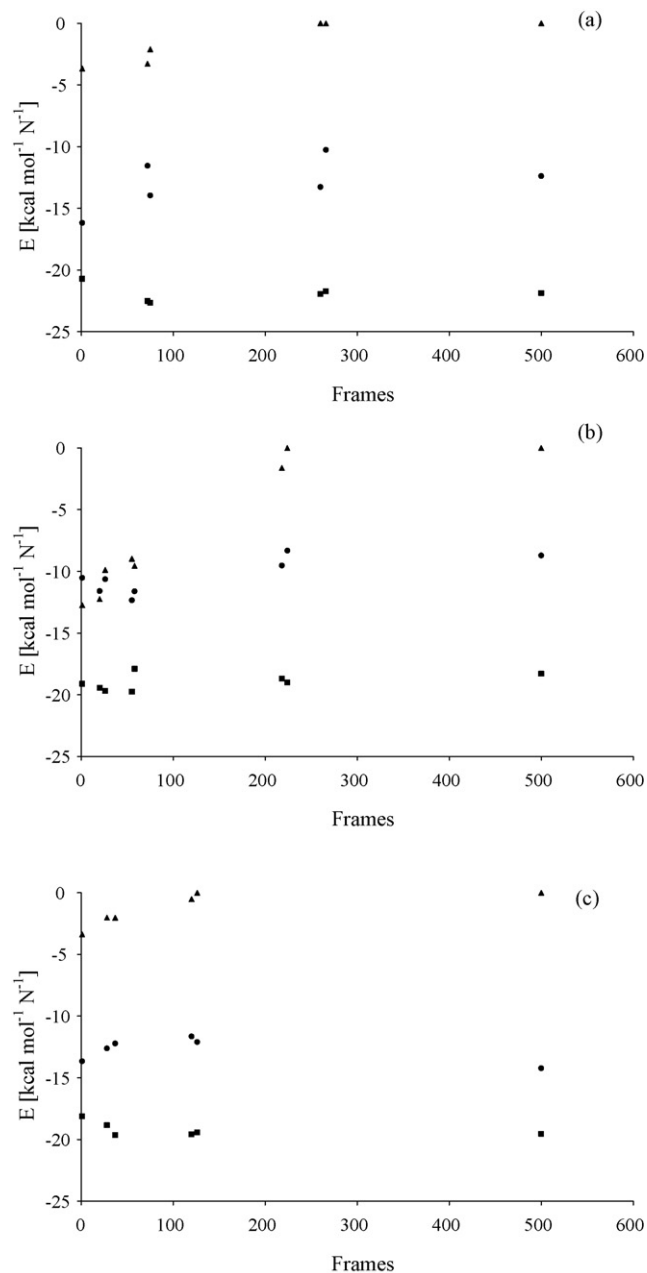**Fig. 5.** Binding energies as a function of time frames for NVE MD simulations at $P_{(H_2S)} = 50$ Pa; (a) 1/3 loading, (b) 2/3 loading, (c) full loading; (●) H_2S, (■) CO_2, (▲) CH_4.

events of CH_4 exiting, in the absence of other event which might influence this process (e.g. simultaneous exiting of more than one molecule or different molecules). Thus we could calculate the binding energy differences (BED) for all considered exiting events, as

$$BED = E_{BIND,after} - E_{BIND,before} \qquad (4)$$

where $E_{BIND,after}$ and $E_{BIND,before}$ are the binding energies for CH_4 or H_2S, calculated immediately after (when CH_4 molecules are far

Table 4
Mean values of BED for H_2S and CH_4 for exiting events and standard deviations

Molecule	BED (kcal/mol)	Standard deviation (kcal/mol)
CH_4	2.816	0.889
H_2S	−2.051	1.950

from zeolite boundaries more than 12.5 Å) and before (when CH_4 molecules are still crossing zeolite boundaries) the CH_4 exit.

Although variations are quite high, due to the complexity of the system and the different composition and loading for each set of simulation, there is a clear trend in binding energy modifications after CH_4 exits. After each escape event, as expected, CH_4 binding energy decreases as absolute value, but this phenomenon involves also a decrease in H_2S binding energy, even though the phenomenon is limited in time. This is probably due to the re-equilibration of the NVE system after a few ps. The behavior testifies that CH_4 molecules tend to exit because of the lower intermolecular attractive forces with the rest of the system; moreover, CH_4 exits seem also to favor the re-allocation of H_2S molecules in adsorption sites, contributing to improve their stability in the framework immediately after each CH_4 exit event.
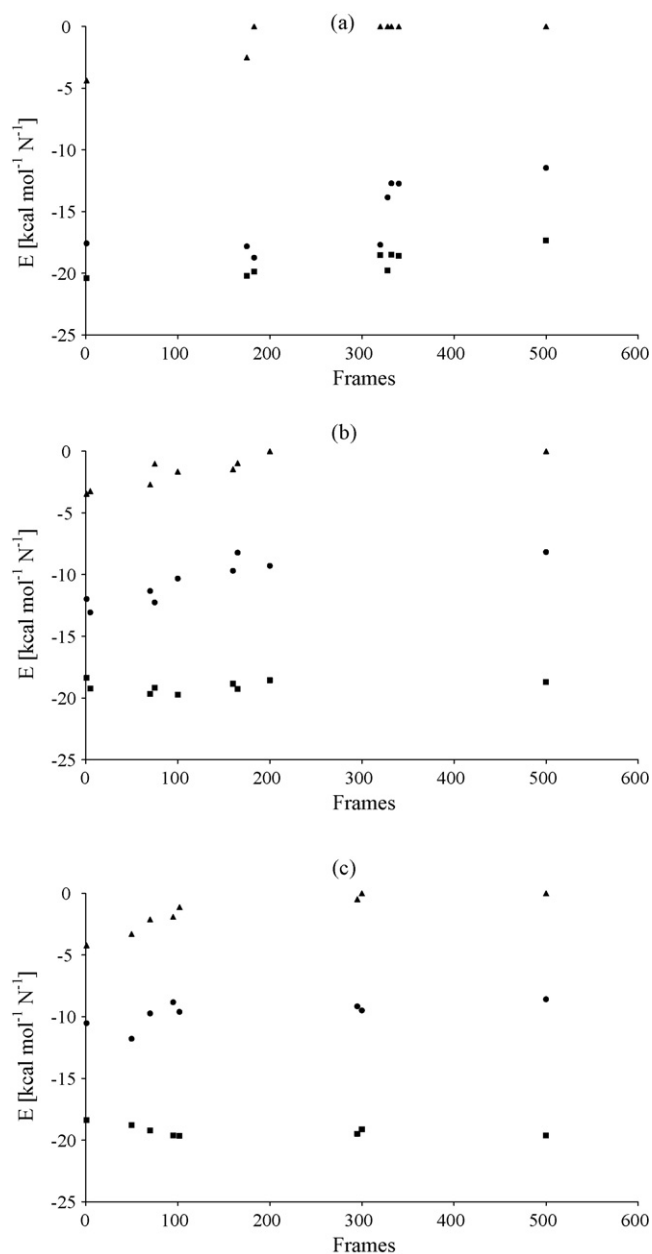
Fig. 6. Binding energies as a function of time frames for NVE MD simulations at $P_{(H_2S)} = 100\,Pa$; (a) 1/3 loading, (b) 2/3 loading, (c) full loading; (●) H_2S, (■) CO_2, (▲) CH_4.

4. Conclusions

In this paper results from GCMC simulations have been coupled, and than compared, with MM/MD simulations for a deeper investigation about adsorption selectivity of zeolite NaY towards H_2S in a biogas mixture. This procedure allowed us to explain the dynamic behavior from a deterministic point of view. Polar H_2S has much more affinity to the hydrophilic zeolite framework than CH_4; this is testified by the relative rapid exit of CH_4 in favor of new H_2S molecules approaching and entering the zeolite cell. CO_2 molecules, essentially by virtue of their linear shape and their quadrupole moment, remain in the pores oscillating around their adsorption sites. Generally speaking, the loading and the composition of the biogas influence the exit events; this is mainly caused by the different number and type of molecules inserted in the cell. The overall

behavior of the system explains results arisen from GCMC simulations, where adsorption of H_2S is favored over CH_4 when $P_{(H_2S)}$ is increasing.

Appendix A. Supplementary data

Supplementary data associated with this article can be found, in the online version, at doi:10.1016/j.cej.2008.08.013.

References

[1] U. Marchaim, Biogas Technology as an Environmental Solution to Pollution, Bull. FAO Agric. Services, Rome, Italy, 1992.
[2] R.E. Speece, Anaerobic Biotechnology for Industrial Wastewaters, Archae Press, Nashville, Tennessee, U.S.A., 1996.
[3] G. Lettinga, A.F.M. van Velsen, S.W. Hobma, W. de Zeeuw, A. Klapwijk, Use of the upflow sludge blanket (USB) reactor concept for biological wastewater treatment, Biotechnol. Bioeng. 22 (1980) 699–734.
[4] A.J. Cruz, J. Pires, A.P. Carvalho, M. Brotas de Carvalho, Physical adsorption of H_2S related to the conservation of works of art: the role of the pore structure at low relative pressure, Adsorption 11 (2005) 569–576.
[5] C.L. Garcia, J.A. Lercher, Adsorption of hydrogen sulfide on ZSM 5 zeolites, J. Phys. Chem. 96 (5) (1992) 2230–2235.
[6] S. Yasyerli, I. Ar, G. Dogu, T. Dogu, Removal of hydrogen sulfide by clinoptilolite in a fixed bed adsorber, Chem. Eng. Process. 41 (9) (2002) 785–792.
[7] H.Y. Young, K. Yang, W.H. Young, K. Seff, Crystal structure of a hydrogen sulfide sorption complex of zeolite LTA, Zeolites 17 (5–6) (1996) 495–500.
[8] X. Xiaochun, I. Novochinskii, C. Song, Low-temperature removal of H_2S by nanoporous composite of polymer-mesoporous molecular sieve MCM-41 as adsorbent for fuel cell applications, Energy Fuels 19 (5) (2005) 2214–2215.
[9] U.S. Environmental Protection Agency, Clean Air Technology Center, Technical Bulletin, Choosing an adsorption system for VOC: carbon, zeolite or polymers? U.S. Environmental Protection Agency, Research Triangle Park, North Carolina, USA, 1999.
[10] J.-C. Charpentier, The Triplet 'Molecular Processes–Product–Process' engineering: the future of chemical engineering? Chem. Eng. Sci. 57 (2002) 4667–4690.
[11] R. Millini, Application of modeling in zeolite science, Catal. Today 41 (1–3) (1998) 41–51.
[12] P. Cosoli, M. Ferrone, S. Pricl, M. Fermeglia, Grand Canonical Monte-Carlo simulations for VOCs adsorption in non-polar zeolites, Int. J. Environ. Technol. Manage. 7 (1–2) (2007) 228–243.
[13] P. Cosoli, M. Ferrone, S. Pricl, M. Fermeglia, Hydrogen sulphide removal from biogas by zeolite adsorption. Part I. GCMC molecular simulations, Chem. Eng. J. 145 (1) (2008) 86–92.
[14] N. Metropolis, A.W. Rosenbluth, N. Rosenbluth, A.H. Teller, E. Teller, Equation of state calculations by very fast computing machines, J. Chem. Phys. 21 (1953) 1087–1092.
[15] A.R. George, C.M. Freeman, C.R.A. Catlow, A computational investigation of zeolite-chlorofluorocarbon interactions, Zeolites 17 (5) (1996) 466–472.
[16] J.-M. Leyssale, G.K. Papadopoulos, D.N. Theodorou, Sorption thermodynamics of CO_2, CH_4, and their mixtures in the ITQ-1 zeolite as revealed by molecular simulations, J. Phys. Chem. B 110 (45) (2006) 22742–22753.
[17] B. Smit, R. Krishna, Molecular simulations in zeolitic process design, Chem. Eng. Sci. 58 (3–6) (2003) 557–568.
[18] S.R. Jale, M. Bülow, F.R. Fitch, N. Perelman, D. Shen, Monte Carlo simulation of sorption equilibria for nitrogen and oxygen on LiLSX zeolite, J. Phys. Chem. B 104 (22) (2000) 5272–5280.
[19] T.J. Hou, L.L. Zhu, X.J. Xu, Adsorption and diffusion of benzene in ITQ-1 type zeolite: Grand Canonical Monte Carlo and molecular dynamics simulation study, J. Phys. Chem. B 104 (39) (2000) 9356–9364.
[20] M. Heuchel, R.Q. Snurr, E. Buss, Adsorption of CH_4–CF_4 mixtures in silicalite: Simulation, experiment, and theory, Langmuir 13 (1997) 6795–6804.
[21] R.L. June, A.T. Bell, D.N. Theodorou, Molecular dynamics study of methane and xenon in silicalite, J. Phys. Chem. 94 (21) (1990) 8232–8240.
[22] G. Sastre, A. Corma, Ordinary diffusion and single file diffusion in zeolites with monodimensional channels. Benzene and n-butane in ITQ-4 and L zeolites, Top. Catal. 24 (1–4) (2003) 7–12.
[23] G. Sastre, C.R.A. Catlow, A. Corma, Influence of the intermolecular interactions on the mobility of heptane in the supercages of MCM-22 zeolite. A molecular dynamics study, J. Phys. Chem. B 106 (5) (2002) 956–962.
[24] http://www.iza-structure.org/databases/.
[25] M.J. Sanborn, R.Q. Snurr, Predicting membrane flux of CH_4 and CF_4 mixtures in faujasite from molecular simulations, AIChE J. 47 (2001) 2032–2041.
[26] R. Nagumo, H. Takaba, S. Suzuki, S. Nakao, Estimation of inorganic gas permeability through an MFI-type silicalite membrane by a molecular simulation technique combined with permeation theory, Micropor. Mesopor. Mater. 48 (1) (2001) 247–254.
[27] R.Q. Snurr, J. Karger, Molecular simulations and NMR measurements of binary diffusion in zeolites, J. Phys. Chem. B 101 (33) (1997) 6469–6473.

[28] S.M. Auerbach, N.J. Henson, A.K. Cheetham, H.I. Metiu, Transport theory for cationic zeolites: diffusion of benzene in Na–Y, J. Phys. Chem. 99 (1995) 10600–10608.

[29] S.G. Charati, S.A. Stern, Diffusion of gases in silicone polymers. Molecular dynamics simulations, Macromolecules 31 (1998) 5529–5538.

[30] A.I. Skoulidas, D.S. Sholl, Direct tests of the darken approximation for molecular diffusion in zeolites using equilibrium molecular dynamics, J. Phys. Chem. B 105 (16) (2001) 3151–3154.

[31] N. Karasawa, W.A. Goddard III, Force fields, structures, and properties of poly(vinylidene fluoride) crystals, Macromolecules 25 (1992) 7268–7281.

[32] P. Demontis, G.B. Suffritti, Sorbate-loading dependence of diffusion mechanism in a cubic symmetry zeolite of type ZK4. A molecular dynamics study, J. Phys. Chem. B 101 (30) (1997) 5789–5793.

[33] C.R. Kamala, K.G. Ayappa, S. Yashonath, Distinct diffusion in binary mixtures confined in slit graphite pores, J. Phys. Chem. B 108 (14) (2004) 4411–4421.

[34] P. Demontis, G. Suffritti, Structure and dynamics of zeolites investigated by molecular dynamics, Chem. Rev. 97 (8) (1997) 2845–2878.

[35] W. Shinoda, M. Mikami, T. Baba, M. Hato, Dynamics of a highly branched lipid bilayer: a molecular dynamics study, Chem. Phys. Lett. 390 (2004) 35–40.

[36] G. Tanaka, L.A. Goettler, Preparation and characterization of nylon 66/montmorillonite nanocomposites with co-treated montmorillonites, Polymer 43 (8) (2002) 541–553.

[37] M. Fermeglia, M. Ferrone, S. Pricl, Computer simulation of nylon/organoclay nanocomposites: prediction of the binding energy, Fluid Phase Equilib. 212 (2003) 315–329.

[38] M. Fermeglia, M. Ferrone, S. Pricl, Estimation of the binding energy in random poly (butylene terephtalate-co-thiodiethylene terephtalate) copolyesters/clay nanocomposites via molecular simulation, Mol. Simulat. 30 (2004) 289–300.

[39] R. Toth, A. Coslanich, M. Ferrone, M. Fermeglia, S. Pricl, S. Miertus, E. Chiellini, Computer simulation of polypropylene/organoclay nanocomposites: characterization of atomic scale structure and prediction of binding energy, Polymer 45 (23) (2004) 8075–8083.

[40] R. Toth, M. Ferrone, S. Miertus, E. Chiellini, M. Fermeglia, S. Pricl, Structure and energetics of biocompatible polymer nanocomposite systems: a molecular dynamics study, Biomacromolecules 7 (2006) 1714–1719.